

In Vitro Anticancer Activity and in Vivo Biodistribution of Rhenium(I) Tricarbonyl Aqua Complexes

Kevin M. Knopf,[†] Brendan L. Murphy,[†] Samantha N. MacMillan,[†] Jeremy M. Baskin,^{†,‡,§} Martin P. Barr,[§] Eszter Boros,^{||,‡,§} and Justin J. Wilson^{*,†,§}

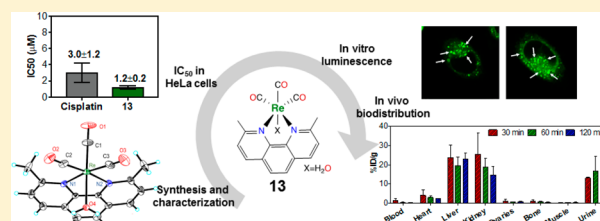
[†]Department of Chemistry & Chemical Biology and [‡]Weill Institute for Cell & Molecular Biology, Cornell University, Ithaca, New York 14853, United States

[§]Thoracic Oncology Research Group, Trinity Translational Medicine Institute, Trinity Centre for Health Sciences, St. James's Hospital and Trinity College Dublin, James's Street, Dublin 8, Dublin, Ireland

^{||}A. A. Martinos Center for Biomedical Imaging, Massachusetts General Hospital, Harvard Medical School, 149 13th Street, Suite 2301, Charlestown, Massachusetts 02129, United States

Supporting Information

ABSTRACT: Seven rhenium(I) complexes of the general formula $fac-[Re(CO)_3(NN)(OH_2)]^+$ where NN = 2,2'-bipyridine (8), 4,4'-dimethyl-2,2'-bipyridine (9), 4,4'-dimethoxy-2,2'-bipyridine (10), dimethyl 2,2'-bipyridine-4,4'-dicarboxylate (11), 1,10-phenanthroline (12), 2,9-dimethyl-1,10-phenanthroline (13), or 4,7-diphenyl-1,10-phenanthroline (14), were synthesized and characterized by ¹H NMR spectroscopy, IR spectroscopy, mass spectrometry, and X-ray crystallography. With the exception of 11, all complexes exhibited 50% growth inhibitory concentration (IC₅₀) values that were less than 20 μM in HeLa cells, indicating that these compounds represent a new potential class of anticancer agents. Complexes 9, 10, and 13 were as effective in cisplatin-resistant cells as wild-type cells, signifying that they circumvent cisplatin resistance. The mechanism of action of the most potent complex, 13, was explored further by leveraging its intrinsic luminescence properties to determine its intracellular localization. These studies indicated that 13 induces cytoplasmic vacuolization that is lysosomal in nature. Additional in vitro assays indicated that 13 induces cell death without causing an increase in intracellular reactive oxygen species or depolarization of the mitochondrial membrane potential. Further studies revealed that the mode of cell death does not fall into one of the canonical categories such as apoptosis, necrosis, paraptosis, and autophagy, suggesting that a novel mode of action may be operative for this class of rhenium compounds. The in vivo biodistribution and metabolism of complex 13 and its ^{99m}Tc analogue 13* were also evaluated in naive mice. Complexes 13 and 13* exhibited comparable biodistribution profiles with both hepatic and renal excretion. High-performance liquid chromatography inductively coupled plasma mass-spectrometry (HPLC-ICP-MS) analysis of mouse blood plasma and urine postadministration showed considerable metabolic stability of 13, rendering this potent complex suitable for in vivo applications. These studies have shown the biological properties of this class of compounds and demonstrated their potential as promising theranostic anticancer agents that can circumvent cisplatin resistance.



INTRODUCTION

Cancer is a leading cause of death worldwide¹ for which chemotherapy remains the most effective strategy for prolonging patient survival. Among the FDA-approved chemotherapeutic agents, the platinum-based drugs cisplatin, carboplatin, and oxaliplatin are especially common and effective, as they are used in approximately 50% of all chemotherapy regimens.² These relatively simple coordination compounds induce their anticancer activity by forming covalent Pt–DNA cross-links,³ which inhibit transcription and give rise to apoptotic cell death.⁴ Despite their widespread use, there are several limitations to the continued implementation of these platinum drugs. For example, they induce toxic side effects, which include nephrotoxicity, ototoxicity, and peripheral neuropathy.⁵ Additionally, after the first-line round of platinum chemotherapy, tumors often relapse in a platinum-resistant

form, which signifies an extremely poor patient prognosis.⁶ Lastly, the platinum drugs are not amenable to detection by in vitro or in vivo imaging. The lack of spectroscopic handles for imaging these compounds in biological settings hinders the possibility of tracking tumor response in vivo and understanding the significance of intracellular localization in vitro.⁷

The exploration of alternative anticancer metal complexes that overcome the limitations associated with platinum drugs is an expanding field of research.⁸ These efforts have led to the development of titanium and ruthenium anticancer agents, some of which have progressed to phase I and II clinical trials.⁸ These advances have provided an impetus for the continued

Received: August 14, 2017

investigation of the periodic table for the discovery of new anticancer drugs.

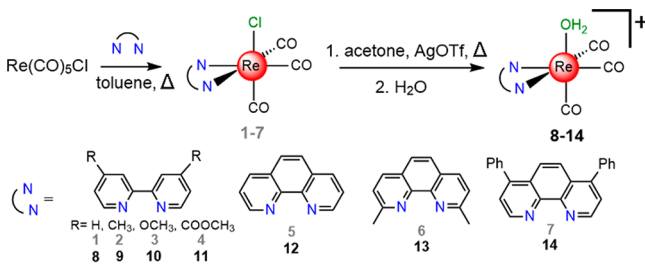
Anticancer applications of rhenium have only recently been explored. These studies have revealed rhenium(I) tricarbonyl complexes to be of particular interest.^{9–33} This class of compounds, most commonly utilized as CO₂ reduction catalysts,³⁴ possess several features that make them amenable for use as anticancer agents. For example, like the platinum-based drugs, they can bind covalently to DNA nucleobases.^{35–38} Furthermore, the ligand substitution kinetics for rhenium(I) tricarbonyl complexes are on the same order of magnitude as those for the platinum-based drugs.³⁹ However, a key advantage of these compounds over conventional platinum anticancer agents is their rich spectroscopic properties that may be leveraged for imaging. The triplet-based luminescent emission of these rhenium(I) tricarbonyl complexes has been successfully used in cellular fluorescence microscopy imaging applications,⁴⁰ and their distinct C≡O stretching frequency enables imaging by vibrational microscopy.⁴¹ Additionally, analogous ^{99m}Tc compounds can be synthesized and used for in vivo SPECT imaging applications.⁴²

In this study, we report a systematic evaluation of a small library of these rhenium(I) tricarbonyl complexes as potential anticancer agents. We have found that these complexes are potent anticancer agents that induce cell death in a manner very different from that of cisplatin. We have also carried out in vivo studies that establish ^{99m}Tc analogues as suitable diagnostic companions for these agents. This study demonstrates that these compounds represent a promising novel class of anticancer agents worthy of continued investigation.

RESULTS

Synthesis and Characterization. The diimine rhenium(I) tricarbonyl complexes were synthesized via previously reported methods (Scheme 1).^{43,44} Treatment of Re(CO)₅Cl with a

Scheme 1. Synthesis of the Rhenium Complexes Investigated in This Study



diimine ligand in refluxing toluene affords the *fac*-[Re(CO)₃(NN)Cl] compounds (1–7), where NN represents the diimine ligand. Because these compounds exhibit poor water solubility, the aqua complexes *fac*-[Re(CO)₃(NN)(OH₂)]⁺ (8–14) were prepared by the treatment of the chlorido complexes with AgOTf in acetone to remove the axial chloride ligand as insoluble AgCl. The resulting triflate complexes were then suspended in water to form the aqua complexes. The enhanced water solubility of the aqua complexes was verified by the fact that we could prepare them as millimolar aqueous solutions, an impossibility for most of the chlorido species.

Complexes 8–14 were characterized by IR spectroscopy (Figure S1, Supporting Information), ¹H NMR spectroscopy (Figures S2–S8), and electrospray ionization mass spectrom-

etry (ESI-MS, Figures S9–S15). Their purity was verified to be greater than 95% by elemental analysis and HPLC. By elemental analysis, the samples were analyzed either as the aqua-triflate salts or as the anhydrous triflate complexes, which may form under vacuum during sample drying. The relative lability of the axial ligand was evidenced by HPLC and NMR spectroscopy. For example, analysis of the chlorido complexes 1–7 by HPLC gives rise to a chromatogram containing two distinct peaks. A representative chromatogram for 5 is shown in the top panel of Figure 1a. By contrast, the chromatograms of

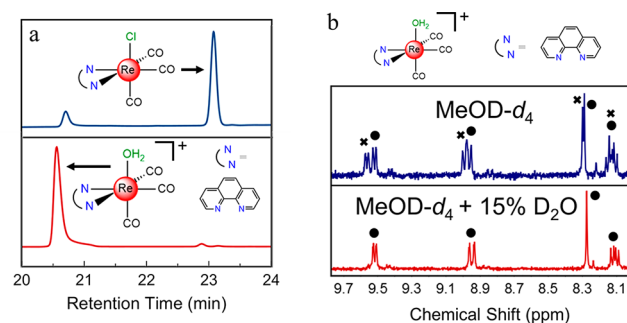


Figure 1. (a) HPLC chromatogram of the phen chlorido species 5 (blue, top trace) and the corresponding aqua species 12 (red, bottom trace) using a methanol gradient elution and monitoring 260 nm. (b) ¹H NMR spectra of the phen aqua species 12 in MeOD-*d*₄ (blue, top trace) and in MeOD-*d*₄ with 15% D₂O (red, bottom trace). The circles designate peaks due to the aqua complex and the x's designate peaks due to the methanol adduct.

the analogous aqua or triflate complexes 8–14 feature a single peak, matching the earlier peak of the chlorido complex, as shown for 12 in the bottom of Figure 1a. Hence, the more lipophilic peak of the chlorido complex is attributed to the intact chloride-bound compound in equilibrium with the aquated species, which has the same retention time as the cationic complex. The HPLC analysis of related rhenium and technetium chlorido complexes also shows two distinct peaks in the HPLC chromatogram, presumably arising from the same phenomenon described here.^{45,46} The ¹H NMR spectra of the cationic complexes 8–14 also reveal a solution equilibrium. Acquisition of these spectra in MeOD-*d*₄ shows the presence of signals for two distinct complexes (Figure 1b). The addition of D₂O to these samples leads to a coalescence of the signals. Therefore, we hypothesize that in MeOD-*d*₄ solution these compounds comprise an equilibrium mixture of axial-bound MeOD-*d*₄ and D₂O complexes; the addition of D₂O acts to drive the equilibrium exclusively to the aqua complex. As such, NMR spectra reported in the experimental section (Supporting Information) for these complexes were acquired in a mixture of MeOD-*d*₄ and D₂O.

Single-Crystal X-ray Diffraction. Single crystals of 11 and 13, as well as derivatives of 9 and 10 with the triflate ion substituted for a nitrate (9-NO₃) and tetrafluoroborate (10-BF₄) counterion, were obtained and analyzed by single-crystal X-ray diffraction to determine their molecular structures (Figure 2). Selected interatomic distances and angles are presented in Table 1. The diimine rhenium tricarbonyl core is maintained in all four structures, but each structure bears different axial ligands. The structures of compounds 9-NO₃ and 11 reveal direct coordination of the nitrate and triflate counterions to the rhenium center, whereas 10-BF₄ and 13 display coordination of the solvent (acetonitrile and water,

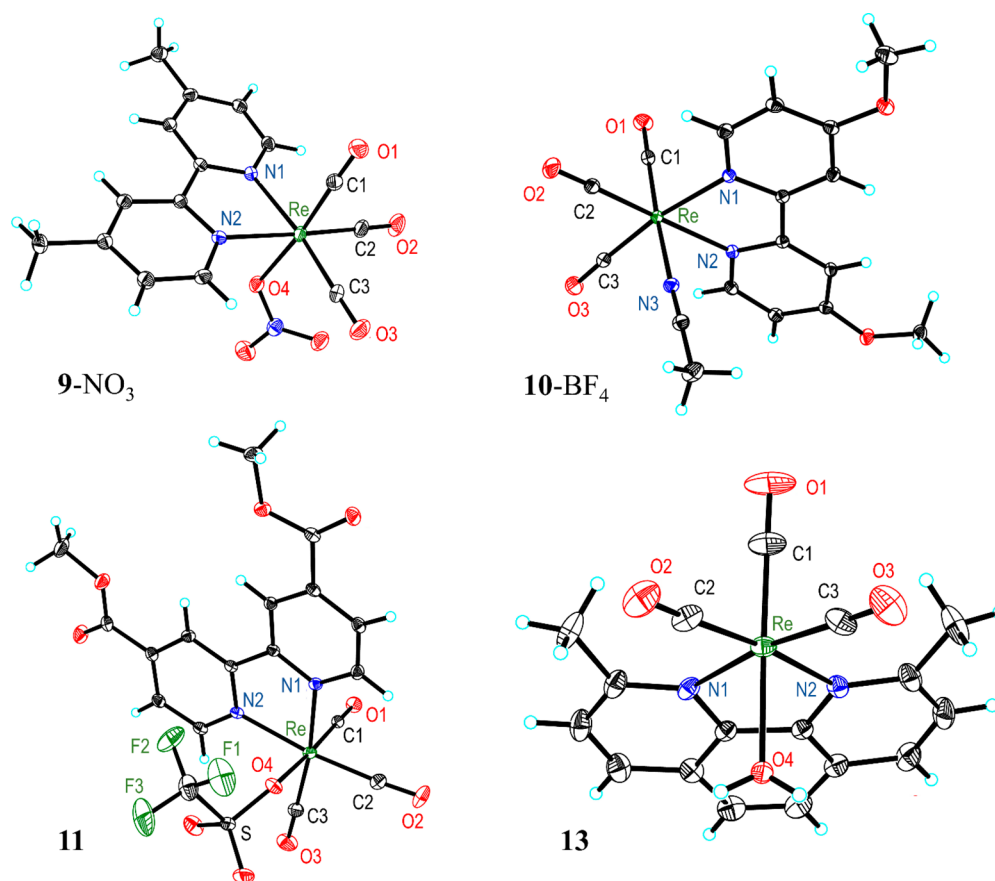


Figure 2. Crystal structures of **9-NO₃**, **10-BF₄**, **11**, and **13**. Outer-sphere solvent molecules and anions are omitted for clarity. Thermal ellipsoids are shown at the 50% probability level.

Table 1. Selected Interatomic Distances (Å) and Angles (deg) from the Crystal Structures Shown in Figure 2^a

	complex			
	9-NO ₃	10-BF ₄	11	13
Re–N1	2.178(4)	2.182(2)	2.180(3)	2.210(3)
Re–N2	2.178(4)	2.180(2)	2.175(3)	2.200(3)
Re–X	2.154(4)	2.149(2)	2.191(2)	2.196(2)
Re–C1	1.899(6)	1.917(3)	1.896(3)	1.896(4)
Re–C2	1.915(6)	1.927(3)	1.921(4)	1.929(4)
Re–C3	1.916(6)	1.929(3)	1.924(4)	1.928(4)
C1–O1	1.163(7)	1.147(3)	1.149(4)	1.147(5)
C2–O2	1.157(7)	1.145(3)	1.154(4)	1.150(4)
C3–O3	1.152(7)	1.144(3)	1.150(4)	1.148(5)
N1–Re–N2	74.60(15)	74.42(7)	75.68(9)	76.18(9)
N1–Re–X	87.73(14)	82.77(8)	79.09(9)	77.99(9)
N1–Re–C1	93.68(19)	94.18(9)	92.69(12)	98.36(15)
N1–Re–C2	99.00(2)	99.72(11)	98.09(13)	100.72(13)
C2–Re–C3	89.0(2)	87.77(13)	89.02(16)	82.84(17)

^aAtom X represents the axial atom, either O4 or N3.

respectively). The direct coordination of a nitrate counterion to related rhenium tricarbonyl diimine complexes is a rare occurrence, as only three such structures are reported;^{47,48} coordination of triflate and acetonitrile is a more common phenomenon.^{49–51} The nature of the axial ligand appears to have a minor influence on the overall interatomic distances of the complexes, as no statistically significant differences are observed.

Given the desired use of these complexes in aqueous solutions, the aqua structure of **13** is of particular interest. The distances and angles found in **13** are similar to those observed in the related 2,2'-bipyridine (bpy) and 1,10-phenanthroline (phen) aqua complexes.^{39,52–55} In platinum anticancer complexes with coordinated water ligands, the Pt–O distance typically ranges from 2.05–2.12 Å.^{56,57} The rhenium aqua compounds have longer Re–O distances of approximately 2.20 Å (2.196 Å in **13**). This slightly longer distance may partly be a consequence of the trans π -accepting CO ligand and a different charge. However, the similarity of the bond lengths between the two types of metal complexes implies the feasibility of using rhenium in place of platinum for biological applications.

The four rhenium complexes adopt similar geometries with fairly consistent interatomic distances and angles. Notably, the C≡O bond lengths are approximately the same among all the complexes. This result is consistent with IR spectroscopy, which also shows that the energies of the C≡O vibrations are invariant between complexes. However, the Re–N distances and N1–Re–N2 bite angle are slightly larger in complex **13** compared to those in the bpy analogues; the Re–N distance is approximately 0.03 Å longer and the N1–Re–N2 angle is 1° wider. This difference is most likely due to the methyl groups on the 2,9-dimethyl-1,10-phenanthroline (dmpen) ligand that sterically crowd the rhenium center, giving rise to elongated interatomic distances. For example, the [Re(phen)-(CO)₃(H₂O)]⁺ complex³⁹ exhibits comparable Re–N distances to the bpy complexes because it does not contain any sterically repulsive methyl groups. By contrast, the crystal structure of

[Re(dmphen)(CO)₃Cl] has Re–N distances that are very close to those found in **13**.⁵⁸

Capacity Factor. The activity of drug candidates may often be correlated to their lipophilicity. The lipophilicity of a class of compounds can be readily compared by determining their retention times on a reverse-phase HPLC column under the same isocratic elution conditions. The capacity factor k , given by the equation⁵⁹ $k = (t_R - t_0)/t_0$, where t_R is the time at which the compound elutes and t_0 is the dead time of the system, is a quantitative measure of retention on a RP-HPLC column that can be correlated directly with the lipophilicity of a compound. As an example, these values were used to determine water–octanol partition coefficients for a library of platinum anticancer agents.⁶⁰

The capacity factors of the rhenium complexes and the isolated diimine ligands are given in Table 2. For these studies,

Table 2. Capacity Factors of Complexes 8–14 and Their Respective Free Ligands on a C18 Column

complex	free ligand capacity factor	aqua complex capacity factor	MeCN complex capacity factor
8	0.42	1.5	3.3
9	0.66	3.3	7.1
10	0.74	3.6	7.2
11	2.4	4.2	8.2
12	0.44	2.1	4.6
13	0.97	4.4	8.9
14	>10	>17	>17

an isocratic elution was used (40:60 MeCN:H₂O, each containing 0.1% TFA). Because MeCN is an effective ligand for rhenium(I), two peaks in the chromatogram were observed, one corresponding to the aqua complex and the other to the MeCN adduct. The peak with the larger capacity factor is assigned to the MeCN adduct, which should be more lipophilic than the aqua complex. As anticipated, functionalization of the diimine gives rise to more lipophilic ligands. The rhenium complexes followed this same trend. Notably, the {Re(CO)₃} core increases the lipophilicity of the complexes relative to the free ligands. The most lipophilic ligand, dpphen, gave rise to the most lipophilic rhenium complex **14**, as evidenced by its capacity factor that exceeded 17.

In Vitro Anticancer Activity. The in vitro anticancer activities of cisplatin and complexes **8–14** were evaluated in HeLa cells by the MTT assay. The resulting 50% growth inhibitory concentration (IC₅₀) values are displayed in Figure 3. Representative dose–response curves are shown in Figures S16. All of the compounds except for **11** exhibited anticancer activity at concentrations under 20 μM. Notably, compounds **9** and **10** gave rise to IC₅₀ values of less than 10 μM. The most potent compound screened was **13**. Its low IC₅₀ value (1.2 ± 0.2 μM) indicates that it is more active than the conventional metal-based anticancer drug cisplatin in HeLa cells (3.0 ± 1.2 μM).

The most potent compounds **9**, **10**, and **13** were further investigated in wild-type and cisplatin-resistant matched cervical cancer cell lines KB-3-1 and KBCP20,^{61,62} ovarian cancer cell lines A2780 and A2780CP70,⁶³ and lung cancer cell lines A549, A549 CisR, H460, and H460 CisR.⁶⁴ In all of the cell lines, the rhenium complexes exhibited similar cytotoxic activity, characterized by IC₅₀ values below 20 μM (Table 3, Figures S17–S21). Notably, these rhenium complexes were nearly equally effective in the cisplatin-resistant cell lines. The

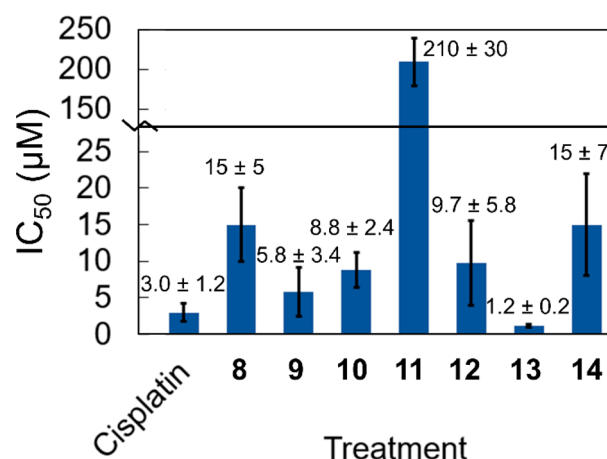


Figure 3. Cell viability data in HeLa cells. The error bars represent one standard deviation from three independent experiments.

resistance factors (RF), the ratio of the IC₅₀ values in cisplatin-resistant and wild-type cells, ranged from 0.6 to 9.4. For comparison, the resistance factor determined for cisplatin was 36 for the A2780 and KB-3-1 cell lines and close to 4 for both the A549 and H460 cell lines. Complexes **9**, **10**, and **13** all exhibited resistance factors lower than that for cisplatin for the given matched cell lines, indicating that they can overcome cisplatin resistance mechanisms. These compounds were also tested in normal lung fibroblasts (MRC-5) as a representative model for noncancerous cells (Table 3). The IC₅₀ values of the rhenium complexes in these cells were about the same or slightly greater than those in the cancer cell lines. By contrast, cisplatin was more cytotoxic to the MRC-5 cells compared to the rhenium complexes.

Nucleobase and Amino Acid Binding. The reactivity of **13**, the most potent complex, with relevant biomolecules was probed using HPLC. This study was conducted to better understand the origin of in vitro anticancer activity of the rhenium complexes. The reaction of 9-ethylguanine, a small-molecule model for the most reactive nucleobase in RNA and DNA,⁶⁵ was initially evaluated. The reaction of **13** with 9-ethylguanine in pH 7.3 MOPS buffer gave rise to a new lipophilic peak in the HPLC, corresponding to the covalent adduct (Figure 4). Additionally, complex **13** interacted appreciably with *N*-acetylcysteine and *N*-acetylhistidine, models for amino acid residues on proteins. Qualitatively, the reaction of **13** was faster with 9-ethylguanine than either *N*-acetylcysteine or *N*-acetylhistidine. The reactions of **13** with methionine, serine, and glycine were also investigated, but these studies revealed no significant interaction between the rhenium complex and the amino acids.

Fluorescence Microscopy. Diimine rhenium(I) tricarbonyl complexes possess a luminescent triplet MLCT excited state that typically emits photons in the yellow region (560–590 nm) of the visible spectrum. These complexes have been successfully utilized for intracellular imaging applications^{27,66–69} via fluorescence microscopy. The ability to image the intracellular localization of the most potent rhenium complex **13** by confocal fluorescence microscopy was investigated. HeLa cells were treated with **13** and incubated for 4 or 24 h prior to imaging. The emission of **13** was detectable well above the background autofluorescence within the cells (Figure 5). The yellow emission of the rhenium was distributed throughout the cytosol. Notably, cytoplasmic vacuoles were observed, an

Table 3. Cell Viability Data in KB-3-1, KBCP20, A2780, A2780CP70, A549, A549 CisR, H460, H460 CisR, and MRC-5 Cells (error represents one standard deviation)

cell line	IC ₅₀ (μM) or RF ^a of complex			
	cisplatin	9	10	13
KB-3-1	1.0 ± 0.3	4.3 ± 1.6	0.77 ± 0.17	0.92 ± 0.20
KBCP20	36 ± 7	5.3 ± 2.1	7.2 ± 1.2	1.6 ± 0.4
RF ^a (KB-3-1)	36	1.2	9.4	1.7
A2780	0.23 ± 0.07	3.5 ± 2.8	2.2 ± 1.8	2.2 ± 0.2
A2780CP70	8.2 ± 1.8	4.7 ± 1.4	2.8 ± 2.5	3.0 ± 0.7
RF ^a (A2780)	36	1.3	1.3	1.4
A549	3.0 ± 1.8	5.2 ± 4.0	9.7 ± 4.1	6.7 ± 4.9
A549 CisR	12.4 ± 8.5	3.9 ± 4.6	5.7 ± 1.8	5.4 ± 1.8
RF ^a (A549)	4.1	0.8	0.6	0.8
H460	0.75 ± 0.43	14 ± 1	9.0 ± 5.0	4.5 ± 0.7
H460 CisR	3.4 ± 1.6	21 ± 12	8.0 ± 2.1	5.3 ± 2.9
RF ^a (H460)	4.5	1.5	0.9	1.2
MRC-5	0.43 ± 0.14	10.7 ± 0.5	6.0 ± 1.9	4.1 ± 0.9

^aRF is the resistance factor, which is the IC₅₀ in the cisplatin-resistant cell line divided by the IC₅₀ in the nonresistant matched cell line.

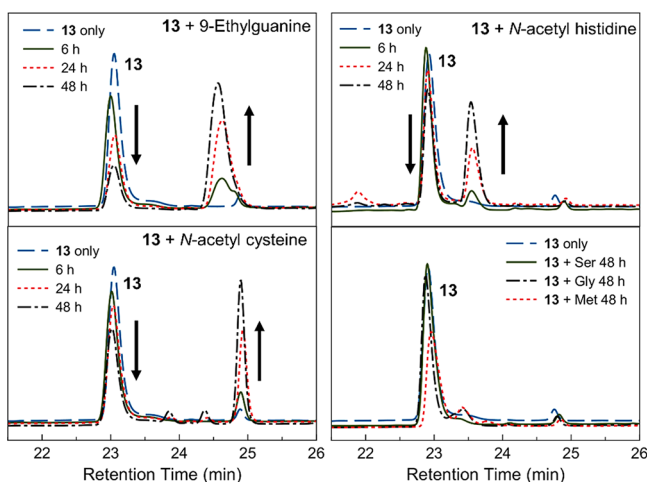


Figure 4. HPLC traces of the reaction of **13** with 9-ethylguanine, *N*-acetylcysteine, *N*-acetylhistidine, or amino acids (serine, glycine, and methionine) for the indicated time monitored at 260 nm.

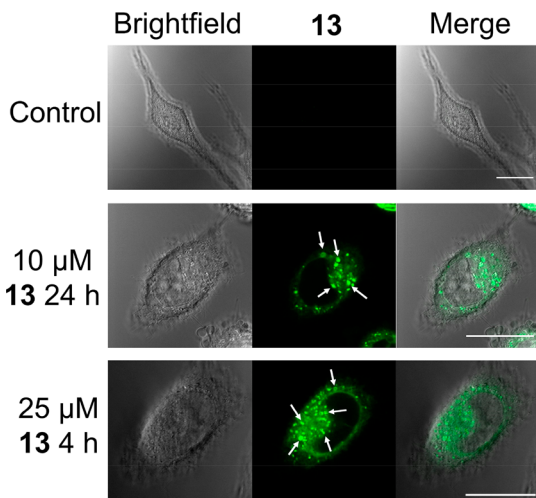


Figure 5. Brightfield and confocal fluorescent microscope images of control HeLa cells and HeLa cells treated with **13**. Arrows point to vacuoles induced by **13** treatment. Scale bars = 20 μm.

apparent effect of the rhenium complex. The outer membranes of these vacuoles were brightly luminescent, indicating a large accumulation of the rhenium complexes.

To further explore the localization of the rhenium complexes, HeLa cells were treated with **13** and different organelle-localizing dyes or transfected to express organelle-specific proteins fused with a fluorescent protein (Figure 6 and Figures S22–S24). These colocalization studies readily reveal that **13**

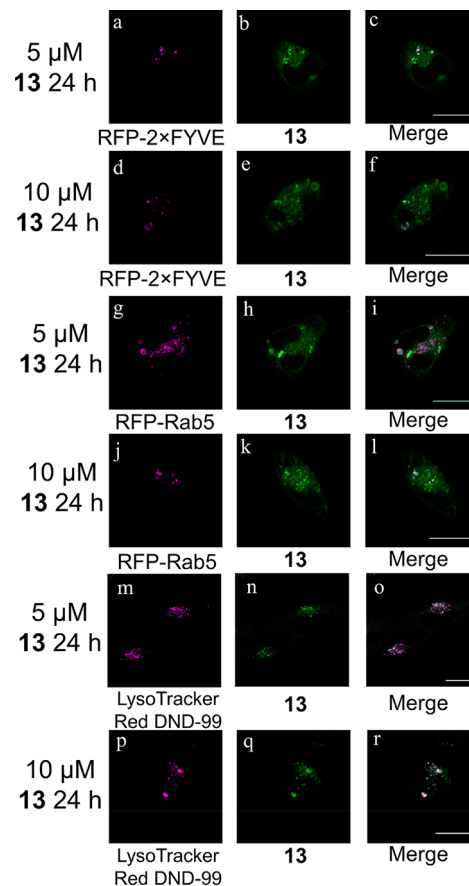


Figure 6. Confocal fluorescent microscope images of HeLa cells treated with **13** and transfected or stained with the indicated plasmid or dye. Scale bars = 20 μm.

does not accumulate in the nucleus, mitochondria, or endoplasmic reticulum (Figure S23). In addition to its cytosolic distribution, the rhenium complex localizes to the large cytoplasmic vacuoles. The nature of these vacuoles was probed by transfecting the cells to express RFP-Rab5 and RFP-2×FYVE fusion proteins. Rab5 is a GTPase that localizes to the outer membrane of the early endosomes,⁷⁰ and 2×FYVE is a tandem arrangement of a protein domain that binds to the lipid phosphatidylinositol 3-phosphate (PI3P),⁷¹ which is highly abundant in early endosomes and in the internal vesicles of multivesicular endosomes. The fluorescence microscopy images indicate that **13** colocalizes with RFP-Rab5, and partially with the RFP-2×FYVE conjugate (Figure 6). This observation suggests that **13** accumulates in some populations of endosomes and further implies that the cytoplasmic vacuoles are endosomal in origin. The lysosomal marker LysoTracker Red DND-99 was also employed. The fluorescent images indicate that the intracellular localization of **13** also correlates strongly with the lysosomes (Figure 6). This result suggests that the vacuoles also have lysosomal character and may be part of a compromised endosome–lysosome fusion process,^{72,73} or that **13** marks a broad population of endosomes and lysosomes. The cells were also transfected to express an RFP-LC3 fusion protein. LC3 is a protein that accumulates on autophagosomes, digestive double-membrane vacuoles that occur during the process of autophagy. Fluorescence microscopy images (Figure S24) indicate that the cytoplasmic vacuoles induced by **13** are not autophagosomes.⁷⁴

Cell Cycle Analysis. Anticancer agents often interfere with the cell cycle. The extent and nature of the cell cycle interruption may be indicative of the agent's mechanism of action.⁷⁵ The relative populations of cells in different phases of the cell cycle can be determined by fixing them, treating them with the fluorescent dye propidium iodide (PI), and then analyzing them with flow cytometry. Cells in the G2/M phase contain twice as much DNA as cells in the G1 phase. In the S phase, cells are actively replicating DNA.⁷⁶ After binding DNA, cisplatin is known to stall cells in the S and G2/M phases.⁷⁷ Accordingly, the treatment of HeLa cells with 5 μM cisplatin for either 24 or 48 h (Figure S25) gave results that are consistent with previous studies using this cell line.⁷⁸

The effect of the rhenium complex on the cell cycle was probed by treating HeLa cells with **13** at 1, 5, or 10 μM for either 24 or 48 h (Figure S26). The most significant changes in the cell cycle population are visible at the 10 μM concentration level. After 24 h, 51.6% of the cells are in the G2/M phase, indicating that this compound stalls cells in these phases.

Annexin V/PI Assay. The flipping of phosphatidylserine to the outer leaflet of the cell membrane is a hallmark feature of apoptotic cell death. The protein annexin V binds to extracellular phosphatidylserine with high affinity and specificity. The treatment of cells with annexin V conjugated to a fluorescent dye (annexin V–Alexa Fluor 488) enables the detection of apoptotic cells. This dye can be used in conjunction with PI to selectively label cells with compromised cell membranes, a feature of necrotic cell death.⁷⁹

When HeLa cells were treated with **13** (5 μM), 19% of the total cell population was alive and possessed exposed phosphatidylserine after 24 h. When **13** was administered at a concentration of 10 μM , a greater proportion of cells label positive for PI, indicating that they are nonviable (Figure S27). However, the population of living cells positive for annexin did not increase. This annexin V assay was also conducted in the

presence of the pan-caspase inhibitor Z-VAD-FMK. The inhibitor had no effect on the histogram of **13**-treated cells but was able to reduce the apoptotic population of cells treated with etoposide, a well characterized apoptosis-inducer.⁸⁰

ROS Analysis. Elevated levels of intracellular reactive oxygen species (ROS) often accompanies cell death.⁸¹ The amount of ROS present in cells treated with **13** were analyzed using 2',7'-dichlorofluorescein diacetate (DCFDA) in conjunction with flow cytometry. Upon exposure to ROS, nonemissive DCFDA oxidizes to a brightly fluorescent product. The emission intensity in each cell, therefore, correlates with the amount of ROS present. Treatment of HeLa cells with 0.03% H_2O_2 gave rise to a greater than 30-fold increase in the intracellular ROS. Upon treating HeLa cells with **13**, however, no significant increases (>2-fold) in the intracellular ROS were observed (Figures S28 and S29), indicating that this compound does not induce the formation of ROS.

JC-1 Assay. The depolarization of the mitochondrial membrane potential (MMP) is an event that occurs early during the course of various cell death modes, such as apoptosis⁸² and paraptosis.⁸³ This event leads to the release of cytochrome *c* and apoptosis-inducing factor from the mitochondria.⁸²

HeLa cells were treated with 5 or 10 μM of **13**, and the depolarization of the MMP was assessed by the JC-1 assay (Figures S30 and S31). These results show that compound **13** does not induce depolarization of the MMP, as the percent of JC-1 aggregates is equivalent to that found in the untreated control. By contrast, carbonyl cyanide *m*-chlorophenyl hydrazine (CCCP), a known mitochondrial depolarizer, led to a substantial reduction in the number of JC-1 aggregates, owing to loss of the MMP.

Cell Viability in the Presence of Inhibitors. To gain further insight into the mechanism of cell death induced by **13**, its cytotoxicity in HeLa cells was evaluated in the presence of different chemical inhibitors that are well characterized in their ability to block chemical processes that mediate cell death. The IC_{50} value of **13** did not change in the presence of the autophagy inhibitor 3-methyladenine (Figure S32). This result indicates that **13** most likely does not induce cell death via autophagy. Treatment of the cells with cycloheximide, a protein synthesis inhibitor that prevents the cell death mode known as paraptosis,^{84,85} also failed to protect cells from the cytotoxic effects of **13** (Figure S32). Similarly, the addition of the necroptosis inhibitor necrostatin-1 did not significantly alter the dose–response curves (Figure S32). Because **13** induces cytoplasmic vacuolization that is endolysosomal in nature, the possibility of lysosomal protease-mediated cell death⁸⁶ was investigated by using the protease inhibitor leupeptin.⁸⁷ Likewise, leupeptin conferred no protective effects on the cells. Lastly, the influence of the pan-caspase inhibitor Z-VAD-FMK was investigated (Figure 7 and Figure S33). The IC_{50} value of cisplatin, which induces caspase-dependent apoptotic cell death,⁸⁸ increased by a factor of 4 in the presence of Z-VAD-FMK. By contrast, Z-VAD-FMK had no protective effect on the IC_{50} value of **13**, indicating that this compound gives rise to caspase-independent cell death. The small increase in potency of **13** in the presence of Z-VAD-FMK is consistent with similar observations for compounds that induce caspase-independent cell death.^{89,90}

Western Blot Analysis of Protein Expression. Different cell death pathways give rise to differential enhancement of specific protein expression levels or may induce post-transla-

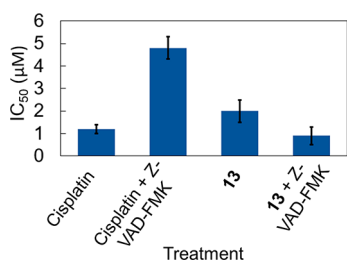


Figure 7. Cell viability in HeLa cells of cisplatin and 13 in the presence and absence of 15 μM of the caspase inhibitor Z-VAD-FMK. Error bars represent one standard deviation.

tional modifications in these proteins. Poly(ADP-ribose) polymerase (PARP), for example, is cleaved by caspases during apoptosis.⁹¹ In addition, the protein LC3 is upregulated during the process of autophagy,⁹² and ERK is phosphorylated (p-ERK) in paraptosis.^{93,94} The expression levels of all of these proteins in HeLa cells were evaluated in the presence of complex 13 by Western blots (Figure S34). This compound did not significantly alter the expression levels of any of these proteins, providing evidence against these mechanisms of cell death. By contrast, cisplatin induced the increase of cleaved PARP levels in a manner that is consistent with the known apoptotic cell death mechanism of this drug.

Cellular Uptake Analysis with Flow Cytometry.

Because most cancer drug targets are intracellular, the cellular uptake of drug candidates may be a determining factor in their *in vitro* or *in vivo* activity. The cellular uptake of 13 was conveniently probed by flow cytometry, leveraging the luminescence properties of the complex for detection (Figures S35–S38).⁹⁵ As the dose concentration of 13 is increased, the intensity of intracellular luminescence measured by flow cytometry also increased (Figure 8a). The cellular uptake scales linearly with the treated concentration up to 50 μM , at which point the uptake begins to level off. Cell uptake of 13 is inhibited when cells are treated at 4 $^{\circ}\text{C}$, and it is reduced upon cotreatment with the endocytosis inhibitor chlorpromazine (Figure 8b). However, uptake is not reduced in the presence of the micropinocytosis inhibitor amiloride (Figure S38). These results implicate active transport of 13 via endocytosis.

NCI-60 Screening. To understand the activity of 13 in comparison to a wide range of validated anticancer drugs, compound 13 was submitted for analysis in the NCI-60 tumor cell panel screen.⁹⁶ In this screening service, the compound is administered in a single-dose of 10 μM to a range of 60

different cancer cell lines. The relative cytotoxicity of a drug candidate in this diverse set of cell lines may reveal cancer types that are particularly susceptible to the tested compound. Additionally, the unique spectrum of activity of a given compound may be correlated with other drug candidates within the NCI database. The results of the NCI-60 single-dose screen are shown in Figure S39. They reveal that 13 is highly effective in all leukemia cell lines tested. This compound also exhibits potent activity in the lung cancer cell line NCI-H522, the melanoma cell line LOX IMVI, and the triple negative breast cancer cell line MDA-MB-468. The COMPARE algorithm, which quantitatively correlates activity spectra in the 60 cell lines of different drug candidates, was carried out for 13. These results are shown in Table 4. The similarity between

Table 4. COMPARE Analysis Results for 13 Based on the NCI-60 Screening Data

Pearson correlation coefficient (PCC)	compound	NSC number
0.649	macbecin II	S330500
0.625	rifamycin SV	S133100
0.605	L-cysteine analogue	S303861
0.585	pibenzimol hydrochloride	S322921
0.572	diglycoaldehyde	S118994
0.572	actinomycin D	S3053
0.557	CHIP (iproplatin)	S256927
0.557	anguidine	S141537
0.550	paclitaxel (taxol)	S125973
0.541	5-azacytidine	S102816

different compounds is given by the Pearson correlation coefficient (PCC); values close to 1 indicate a high degree of similarity between drug candidates. The highest correlations for 13 are the natural products macbecin II (PCC 0.649) and rifamycin SV (PCC 0.625). Notably, the platinum(IV) drug candidate iproplatin⁹⁷ is the only metal-containing compound to correlate with the spectrum of activity of 13.⁹⁸

Synthesis and *In Vivo* Evaluation of the ^{99m}Tc Analogue of 13. Tc is the lighter congener of Re and exhibits similar chemistry. This similarity enables the use of ^{99m}Tc analogues of these rhenium anticancer agents as diagnostic partners for SPECT imaging or biodistribution studies. To assess *in vivo* behavior of 13, we synthesized the ^{99m}Tc analogue 13*. Compound 13* was prepared from the well-known precursor [^{99m}Tc(H₂O)₃(CO)₃]⁺ and the dmphen

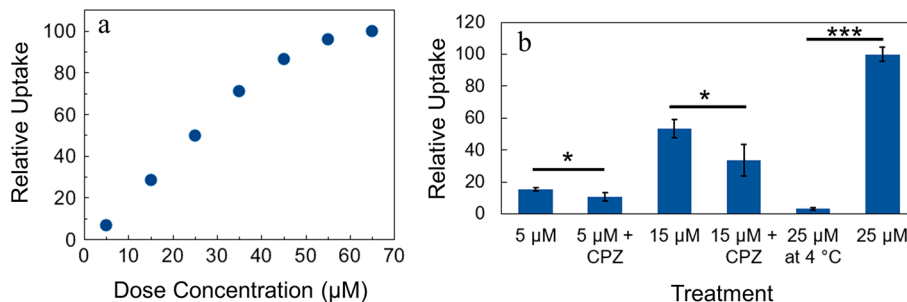


Figure 8. Relative uptake of 13 by investigating (a) dose concentration and (b) mechanism of uptake (all treatments lasted 4 h). For Student's *t*-test analysis, $p < 0.05$ (*) or $p < 0.001$ (***). Error bars represent one standard deviation from three trials. CPZ represents 25 μM chlorpromazine. For the four total 5 μM and 15 μM treatments in part b, propidium iodide was used to gate only live cells because dead cells may have different uptake, and chlorpromazine was somewhat toxic to the cells.

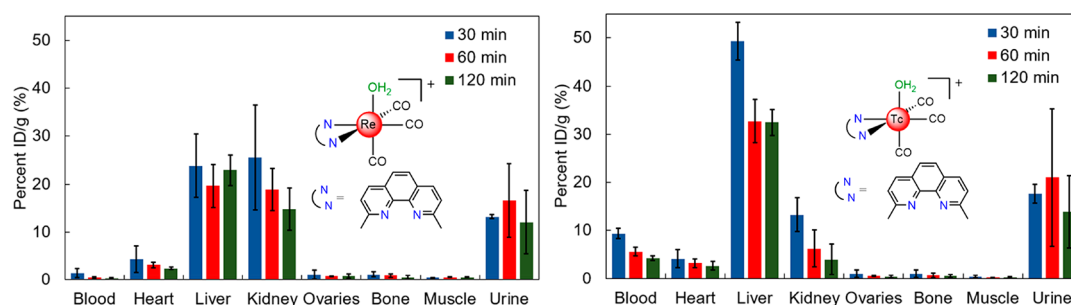


Figure 9. Biodistribution of the Re and ^{99m}Tc tricarbonyl complexes with the dmphen ligand using ICP-MS to detect rhenium and a gamma counter to detect technetium.

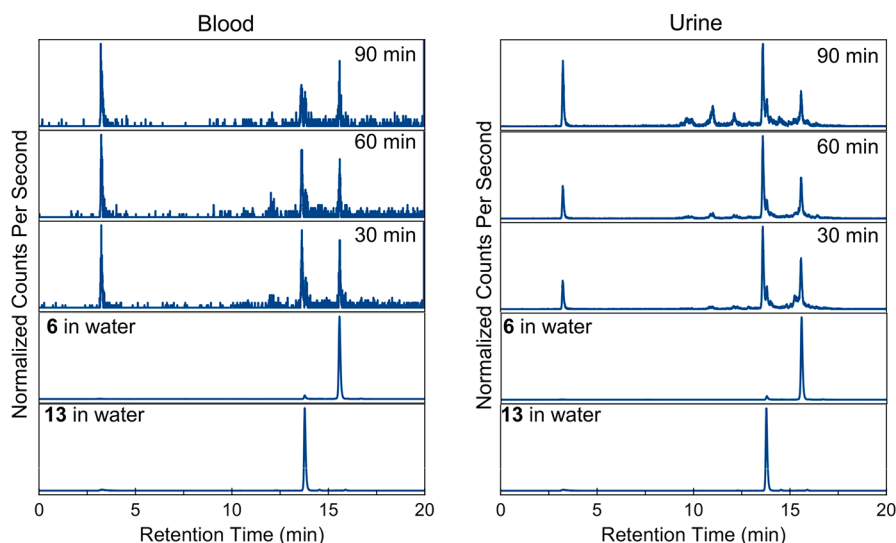


Figure 10. Normalized HPLC-ICP-MS traces of analysis of blood serum (left) and urine (right) of **13** in mice at the indicated time points.

ligand (Figure S40) and purified using preparative HPLC (Figure S41). After removal of the organic solvent, **13*** was reconstituted and administered to naïve C57Bl6 mice via tail vein catheter simultaneously with a 0.10 $\mu\text{mol/kg}$ dose of **13**. Biodistribution was carried out at 30, 60, and 120 min postinjection. Residual activity in select organs, tissues, and fluids (blood, heart, liver, kidney, ovaries, bone, muscle, urine) was quantified (Figure 9 and Table S1). We observed rapid renal and hepatic clearance of **13***. No significant nonspecific uptake was observed in any organs studied, paving the way for future studies of the distribution of **13*** in models of disease.

Biodistribution and Metabolite Analysis of 13. We also assessed biodistribution and the metabolic profile of **13** in naïve C57Bl6 mice. After allowing for decay of ^{99m}Tc, the rhenium concentration in select organs, tissues, and fluids (blood, heart, liver, kidney, ovaries, bone, muscle, urine) was quantified using inductively coupled plasma–mass spectrometry (ICP-MS). Biodistribution of **13** revealed comparable behavior to **13*** in most organs (Figure 9), suggesting the suitability of using the ^{99m}Tc analogue as a diagnostic partner. Notably, **13** exhibits higher uptake in the kidneys and accelerated blood clearance properties compared with those of **13***.

Additionally, fractions of blood plasma and urine from each time point were collected and subjected to analysis using HPLC-coupled ICP-MS detecting Re species (Figure 10). Traces of samples were collected at 30, 60, and 120 min, as well as reference traces of **13** with H₂O as the axial ligand (aqua-) and **6** with Cl[−] as the axial ligand (chlorido-). Both blood

plasma and urine analysis show similar trends. In vivo, a significant fraction of **13** experiences an exchange of the axial aqua ligand to the chloride, as indicated by a shift in retention time from 13.8 to 15.6 min. Furthermore, two distinct metabolite peaks are observed: a hydrophilic species (3.3 min) and a more lipophilic species (13.6 min). At later time points, a relative increase of the hydrophilic species is observed, but both aqua and chlorido species of **13** can be detected in both blood plasma and urine at all time points. The presence of **13** or its chlorido form **6** at all time points suggests that this complex may reach tumor cells in vivo prior to decomposition.

DISCUSSION

Although the platinum-based drugs have been a mainstay in first-line chemotherapy for decades, their toxic side effects and susceptibility to resistance remain significant challenges for their ongoing use in the clinical setting. These limitations have driven the search for alternative metal-based drugs, efforts that have led to the clinical trials of titanium, gallium, and ruthenium complexes.⁸ More recently, complexes of rhenium have emerged as alternatives for the traditional platinum-based drugs.⁹⁹ For example, an increasing number of rhenium compounds with IC₅₀ values under 50 μM in cancer cell lines have been discovered.^{99,100}

In this study, we developed a small library of rhenium(I) tricarbonyl aqua complexes and evaluated their anticancer potential. Structural variety of these complexes was provided by seven different diimine ligands, each bearing functional groups

with different electronic-withdrawing and lipophilic properties (Scheme 1). These compounds were characterized by standard techniques, including ^1H NMR spectroscopy, mass spectrometry, and X-ray crystallography (Figure 2). Both ^1H NMR spectroscopy and HPLC indicate that the axial aqua ligand is relatively labile and subject to substitution with coordinating solvents, such as MeCN, or anions, such as chloride. The aqua ligands were employed to confer increased aqueous solubility to these complexes. However, the aqua ligands also potentially introduce another complication of acid–base chemistry via deprotonation of the coordinated water to form a hydroxide. The ligand substitution kinetics and therefore the biological activity of the aqua and hydroxido species are expected to be substantially different. For the related *fac*- $[\text{Re}(\text{CO})_3(\text{OH}_2)_3]^+$ complex, the $\text{p}K_{\text{a}}$ value of the coordinated water is 7.5.¹⁰¹ Assuming that the rhenium(I) aqua complexes studied here have a similar $\text{p}K_{\text{a}}$ value, the complexes will exist in approximately a 50:50 mixture of the aqua and hydroxido forms at physiological pH. The studies in this manuscript therefore represent the composite effects of these two species under biological conditions.

These compounds were initially screened in HeLa cells (Figure 3). The IC_{50} values of the compounds span a wide range, depending on the nature of the coordinated diimine ligand. Some structure–activity relationships for this class of compounds can be discerned from this study. Namely, compound 11, which bears the diester-bpy ligand, is the least active. Thus, the presence of electron-withdrawing functional groups on the diimine ligand may act to reduce the biological activity of the complex. The lipophilicities of the complexes were determined using HPLC capacity factors to examine its relation to the biological activity as well. The capacity factor of 13 is the second largest among the seven compounds. The most lipophilic compound is 14, which bears the large 4,7-diphenyl-1,10-phenanthroline ligand. The cytotoxicity of 14, however, is substantially diminished relative to that of 13. Therefore, a direct correlation of lipophilicity with anticancer activity is not observed for this class of compounds.

The chlorido complexes bearing bpy (1), phen (5), and dmphen (6) diimine ligands were previously investigated for anticancer activity in PC-3 (prostate cancer), MCF-7 (breast cancer), and H522 (lung cancer) cell lines.^{58,102} Complex 6 was the most active, consistent with our studies of the aqua analogue 13. Notably, the use of the aqua complexes in this study enabled us to dissolve the compounds in pure water prior to dissolution in culture medium. By contrast, the chlorido analogues were diluted from DMSO stock solutions. Because the presence of DMSO may alter the biological activity of metal-based anticancer agents, caution should be taken when using this solvent for any new class of compounds.^{103,104}

On the basis of the initial screening in HeLa cells, the most active compounds, 9, 10, and 13, were further evaluated in cisplatin-resistant cell lines. Because platinum resistance represents a significant problem in the clinic, the development of new metal-based drugs that are not cross-resistant to cisplatin is of significant importance. Cisplatin was 36 times less effective in resistant ovarian cancer (A2780CP70)⁶³ and cervical cancer (KBPC20)^{61,62} cell lines compared to the parental wild-type cell lines (Table 3). Additionally, in the lung cancer cell lines, cisplatin was 4.1 times less effective in resistant A549 cells and 4.5 times less effective in resistant H460 cells.⁶⁴ By contrast, the activity of the rhenium complexes in the cisplatin-resistant cell lines was always equivalent to that in the

wild-type cells, with the exception of 10 in KBPC20 cells. These results indicate that this class of rhenium complexes can broadly circumvent platinum resistance mechanisms in a wide range of cancer types. Platinum resistance is multifactorial, entailing decreased drug uptake, increased glutathione production, and increased DNA repair capacity.^{63,105,106} The origin of the lack of cross-resistance of the rhenium complexes with cisplatin is not clear, but it suggests that these rhenium complexes are operating by different mechanisms of action. Noncancerous MRC-5 lung fibroblasts were used as a model for healthy cells. The cytotoxic activities of 9, 10, and 13 in this cell line were typically 2–4 fold lower than in HeLa, KB-3-1, and A2780 cells but possessed similar toxicity in A549 and H460 cells. For comparison, cisplatin was about 2–7 times more cytotoxic in MRC-5 cells than in the HeLa, A549, and H460 cancer cell lines. This result suggests that this rhenium compound class may possess favorable therapeutic indices for further in vivo applications.

The interaction of the most potent complex, the dmphen aqua complex 13, with relevant biological nucleophiles, was explored to investigate potential biological targets. Metal complexes typically bind to guanine in RNA or DNA, or amino acids such as histidine and cysteine.¹⁰⁷ By HPLC, 13 has high affinity for 9-ethylguanine, *N*-acetylcysteine, and *N*-acetylhistidine but does not show substantial binding to the other amino acids tested including methionine (Figure 4). Notably, 13 binds to 9-ethylguanine more rapidly than to *N*-acetylcysteine and *N*-acetylhistidine. Rhenium(I) tricarbonyl complexes, such as 13, are known to interact with guanine³⁸ in DNA^{35,36} and histidine residues in proteins;^{108–111} the interaction of such complexes with cysteine, however, is less documented.¹¹² These studies suggest that cysteine residues may also be important intracellular targets.

Compound 13 was further investigated to probe its mechanism of action. Using microscopy, cell viability assays, flow cytometry assays, and Western blotting, it was concluded that 13 induces a noncanonical form of cell death. The details of this cell death and its failure to fit well-characterized cell death modes is explained in this section. First, confocal fluorescence microscopy was used to image the yellow $^3\text{MLCT}$ luminescence of 13 directly in living HeLa cells (Figure 5). The fluorescence microscope images reveal that 13 induces cytoplasmic vacuolization and is localized diffusely throughout the cytosol and within the membranes of these vacuoles. Interestingly, no nuclear accumulation is seen despite the similarity of the rhenium complexes to platinum-based drugs in their ability to bind to 9-ethylguanine. Colocalization studies (Figure 6 and Figure S22) with LysoTracker Red DND-99 and the RFP-Rab5 fusion protein suggest that these vacuoles are endolysosomal in origin. The possibility of these vacuoles arising from the endoplasmic reticulum or from autophagosomes during autophagy was ruled out by colocalization studies employing an ER-localizing RFP-STIM1 fusion protein and an autophagosome-localizing RFP-LC3 marker (Figures S23 and S24). The yellow luminescence of 13 present in the vacuoles shows no overlap with either of these markers. Furthermore, microscopy images obtained of cells treated with 13 in the presence of the autophagy inhibitor 3-methyladenine still display the characteristic cytoplasmic vacuolization, further eliminating the possibility of these structures as autophagosomes (Figure S23). Like autophagy, paraptosis is a mode of cell death that proceeds in part via cytoplasmic vacuolization. The vacuoles formed during paraptosis are derived from the

ER.⁸⁴ On the basis of the negative result for colocalization with the RFP-STIM1 fusion protein, paraptosis as a mechanism of cell death may be ruled out as well. Additionally, treatment of the cells with the protein synthesis inhibitor cycloheximide or the Ca²⁺ channel inhibitor 2-aminoethoxydiphenyl borate, which are both known to inhibit paraptosis,⁸⁴ failed to prevent formation of the vacuoles upon exposure to **13**. These results further confirm that the cytoplasmic vacuolization does not arise from the induction of paraptosis.

The mechanism of cell death was also investigated by evaluating the cytotoxicity of **13** in the presence of various cell death inhibitors. Consistent with the imaging studies described above, 3-methyladenine and cycloheximide had no effect on the cytotoxicity of **13** (Figure S32), further ruling out autophagy and paraptosis as the mechanism of cell death. Because necroptosis, a regulated form of necrosis, was characterized as the cell death pathway induced by rhenium(V)-oxo compounds,⁸⁸ the cytotoxicity of **13** was probed in the presence of the necroptosis inhibitor necrostatin-1. Necrostatin-1 had no effect on the cytotoxic activity of **13**, suggesting that necroptosis is not operative. Because the vacuoles induced by **13** are endolysosomal in origin, the possibility of cell death induced by lysosomal proteases was investigated with the serine and cysteine protease inhibitor leupeptin. Again, no decrease in the cytotoxic effects of **13** was observed in the presence of this protease inhibitor. Caspases are proteases that regulate programmed cell death. Their activation is implicated in apoptosis, and their downregulation in cancer cells has been linked to drug resistance. The use of the pan-caspase inhibitor Z-VAD-FMK revealed that **13** retains its cytotoxicity when caspases are inhibited and therefore induces cell death in a caspase-independent manner (Figure 7).

Western blots were performed to evaluate protein expression levels that might be altered by different cell death modes. A Western blot for PARP and cleaved PARP in HeLa cells treated with **13** showed no significant alteration of the expression levels of these proteins, further ruling out apoptosis (Figure S34). Levels of LC3 were also unaffected by **13**, indicating that autophagy was not operative. Western blots for ERK and p-ERK, proteins activated from ER stress related to paraptosis,⁹⁴ showed no change in expression level either. These studies validate the novel mode of cell death induced by **13**.

Further studies were carried out to investigate the potential role of ROS and depolarization of the MMP in mediating the cell death induced by **13**. Compound **13** did not lead to an increase in intracellular ROS (Figures S28 and S29) nor did it depolarize the MMP (Figures S30 and S31). Compound **13** did give rise to flipping of phosphatidylserine to the outer membrane (Figure S27). Both paraptosis and necrosis give rise to an overproduction of ROS within the cell^{113–116} and apoptosis is known to depolarize the MMP.^{117,118} Thus, the cell death mechanism of **13** does not categorically fit within any of these descriptions. Although the flipping of phosphatidylserine is usually associated with apoptosis, alternative forms of cell death such as necrosis may also give rise to this phenomenon.¹¹⁹ Therefore, although **13** produces a small population of annexin-positive living cells, it is not caused by apoptosis based on the other assays showing nonapoptotic characteristics of cell death. Additionally, the annexin/PI histogram of **13** is much different than that of etoposide, a known apoptosis-inducer.

Cell cycle analysis indicates that **13** arrests cells in the G2/M phases (Figure S26), implying that it may have antimetastatic effects. Anticancer drugs such as celastrol⁹³ and taxol¹²⁰ also

inhibit cells in these phases. By contrast, cisplatin, a DNA-binding agent, inhibits cells predominantly in the S-phase (Figure S25).

Thus far, there have been few studies that investigate the mechanism of cell death induced by potential rhenium anticancer agents. These investigations reveal a diverse range of pathways possible for these compounds. Bis(quinoline) rhenium(I) tricarbonyl complexes give rise to both apoptosis and necrosis.^{24,26} A diimine rhenium(I) tricarbonyl complex designed as a histone deacetylase inhibitor induces paraptosis.¹⁵ Rhenium N-heterocyclic carbene complexes induce caspase-independent cell death associated with cell cycle arrest, similar to **13**.⁹ Higher oxidation state rhenium complexes have also been investigated, namely rhenium(IV) compounds bearing a chelating diimine and four chloride ligands that kill cells via apoptosis,¹²¹ and rhenium(V) oxo complexes that give rise to necroptosis, a regulated form of necrosis.⁸⁸ Despite the array of investigations carried out in this work, the cell death mechanism for **13** remains uncertain. It is possible that **13** gives rise to an as-of-yet uncharacterized mode of cell death. The implications of this feature for the potential use of **13** as an anticancer drug are uncertain, but the fact that this compound is able to circumvent cisplatin resistance and kill cells independently of caspase function suggests its potential in anticancer therapy.

The cellular uptake of **13** was investigated using flow cytometry, capitalizing on its inherent luminescence properties. The cellular uptake of **13** exhibits saturation behavior at high concentrations and is substantially decreased at 4 °C (Figure 8). These results collectively indicate that **13** enters cells via active transport. This result is also consistent with the lack of correlation of the cytotoxicity with lipophilicity, as this correlation holds primarily for compounds that enter cells via passive diffusion. Treatment of cells with the clathrin-coated pit endocytosis inhibitor chlorpromazine¹²² decreased cell uptake, further suggesting that **13** is taken up via endocytosis. This result is significant because the confocal fluorescence microscope images indicate that **13** localizes to the enlarged endolysosomes. These enlarged vacuoles may therefore be a consequence of the endocytotic uptake of **13**. The mechanism of cell uptake has been explored for several related rhenium complexes. Rhenium compounds decorated with fructose, for example, are taken up actively by a fructose transporter.²⁸ Similarly, a glucose analogue enters the cells via the GLUT transporter.¹²³ A hydroxamic acid-functionalized rhenium tricarbonyl complex is taken up via an active but non-endocytotic pathway.¹⁵ The results determined here for **13**, which bears no additional targeting group, suggest that endocytotic uptake may be the default uptake pathway for such rhenium(I) tricarbonyl complexes.

The NCI-60 screening results used in conjunction with the COMPARE algorithm (Table 4) relates **13** to several organic natural products. The top correlations arise for macbecin II and rifamycin SV. The lack of any strong correlations with the FDA-approved platinum-based drugs confirm that **13** acts via a very different mechanism of action. Macbecin II is a well-characterized inhibitor of heat shock protein 90 (Hsp90),¹²⁴ and rifamycin SV is an inhibitor of DNA-dependent RNA polymerase.¹²⁵ Hsp90 is a highly abundant cytosolic protein that is involved in protein folding.¹²⁶ It is overexpressed in leukemia and other cancer types¹²⁷ and has recently arisen as a promising drug target.¹²⁸ Notably, rifamycin SV is also known to possess Hsp90 inhibitory properties.¹²⁹ Thus, the high

correlation between macbecin II, rifamycin SV, and **13** suggests that Hsp90 could be a common molecular target.

To validate the potential of this compound for clinical use, the in vivo properties of **13** and its ^{99m}Tc analogue **13*** were investigated to determine the metabolic outcomes of the complexes. When injected simultaneously in the same animal, both complexes exhibit similar profiles in biodistribution studies in mice (Figure 9). This result is somewhat surprising given the much faster ligand substitution kinetics of $\text{Tc}(\text{CO})_3$ complexes compared to $\text{Re}(\text{CO})_3$ complexes¹³⁰ but bodes well for the potential use of ^{99m}Tc analogues as diagnostic partners. Consistent with previous studies on $^{99m}\text{Tc}(\text{CO})_3$ complexes,^{131,132} both compounds undergo renal and hepatobiliary modes of excretion, further evidenced by Re and ^{99m}Tc in the urine and liver. Metabolite analysis of **13** using HPLC-ICP-MS reveals the presence of four main Re species at all time points analyzed (Figure 10); in vivo, most of **13** experiences exchange of the axial aqua ligand to chloride, as well as the conversion to two more hydrophilic metabolites of unknown nature. The presence of intact **13** in vivo at all time points suggests that this compound can access tumor sites prior to decomposition. Ongoing studies are aimed at evaluating the in vivo anticancer activity of this novel compound.

CONCLUSION

A systematic study on the anticancer potential of rhenium(I) tricarbonyl complexes was performed. These efforts revealed that this class of compounds exhibit in vitro anticancer activity. Compound **13** was discovered as a new lead candidate, as it is more potent than the established metal-based anticancer drug cisplatin. In addition, this complex overcomes cisplatin resistance and is trackable by luminescence imaging. Its framework also allows for the facile synthesis of the ^{99m}Tc analogue for diagnostic imaging, which has been used in this study to determine biodistribution and will facilitate future in vivo studies. Mechanistic studies on **13** indicate that it induces caspase-independent cell death accompanied by cytoplasmic vacuolization. Categorization of the cell death in one of the canonical modes was unsuccessful, suggesting that **13** may be inducing cytotoxicity via a novel pathway. The molecular target of **13** and related rhenium(I) complexes also remains uncertain. Our current efforts are aimed toward identifying the target of **13** and pursuing the anticancer properties of these compounds within in vivo models.

ASSOCIATED CONTENT

Supporting Information

The Supporting Information is available free of charge on the ACS Publications website at DOI: 10.1021/jacs.7b08640.

Experimental procedures, characterization data, cell viability curves, microscope images, flow cytometry plots and histograms, NCI-60 single-dose mean graph, and crystal data tables (PDF)

Crystallographic data (CIF)

AUTHOR INFORMATION

Corresponding Author

*jjw275@cornell.edu

ORCID

Jeremy M. Baskin: 0000-0003-2939-3138

Eszter Boros: 0000-0002-4186-6586

Justin J. Wilson: 0000-0002-4086-7982

Present Address

#Department of Chemistry, Stony Brook University, Stony Brook, NY 11790-3400.

Notes

The authors declare no competing financial interest.

ACKNOWLEDGMENTS

This work was supported by Cornell University and by the Office of the Assistant Secretary of Defense for Health Affairs through the Ovarian Cancer Research Program under award no. W81XWH-17-1-0097. B.L.M. acknowledges support for undergraduate summer research from the Gerald A. Hill and Kathleen Holmes Hill Fellowship at Cornell. J.M.B. acknowledges support from the National Institutes of Health (R00GM110121). E.B. acknowledges the NHLBI for support (K99HL125728). LCICP instrumentation at Massachusetts General Hospital was funded by NIH, the office of the director (S10OD010650). This work made use of the NMR facility at Cornell University, which is supported by the NSF under award number CHE-1531632. This work also made use of the flow cytometer and Zeiss LSM 880 microscope (NYSTEM CO29155 and NIH S10OD018516) at the Cornell University Biotechnology Resource Center (BRC). We also thank the Hu and Selvaraj laboratories at Cornell University for sharing DNA plasmids and reagents. Ms. Nicole Spiegelman is thanked for assistance with Western blot experiments.

REFERENCES

- (1) Siegel, R. L.; Miller, K. D.; Jemal, A. *CA-Cancer J. Clin.* **2017**, *67*, 7–30.
- (2) Galanski, M. A.; Jakupec, M.; Keppler, B. K. *Curr. Med. Chem.* **2005**, *12*, 2075–2094.
- (3) Jamieson, E. R.; Lippard, S. J. *Chem. Rev.* **1999**, *99*, 2467–2498.
- (4) Todd, R. C.; Lippard, S. J. *Metallomics* **2009**, *1*, 280–291.
- (5) Hartmann, J. T.; Lipp, H.-P. *Expert Opin. Pharmacother.* **2003**, *4*, 889–901.
- (6) Galluzzi, L.; Senovilla, L.; Vitale, I.; Michels, J.; Martins, I.; Kepp, O.; Castedo, M.; Kroemer, G. *Oncogene* **2012**, *31*, 1869–1883.
- (7) Cheff, D. M.; Hall, M. D. *J. Med. Chem.* **2017**, *60*, 4517–4532.
- (8) Ott, I.; Gust, R. *Arch. Pharm.* **2007**, *340*, 117–126.
- (9) Simpson, P. V.; Casari, I.; Paternoster, S.; Skelton, B. W.; Falasca, M.; Massi, M. *Chem. - Eur. J.* **2017**, *23*, 6518–6521.
- (10) Chakraborty, I.; Carrington, S. J.; Roseman, G.; Mascharak, P. K. *Inorg. Chem.* **2017**, *56*, 1534–1545.
- (11) Carreño, A.; Aros, A. E.; Otero, C.; Polanco, R.; Gacitúa, M.; Arratia-Pérez, R.; Fuentes, J. A. *New J. Chem.* **2017**, *41*, 2140–2147.
- (12) Raszeja, L. J.; Siegmund, D.; Cordes, A. L.; Güldenhaupt, J.; Gerwert, K.; Hahn, S.; Metzler-Nolte, N. *Chem. Commun.* **2017**, *53*, 905–908.
- (13) Collery, P.; Santoni, F.; Ciccolini, J.; Tran, T. N. N.; Mohsen, A.; Desmaele, D. *Anticancer Res.* **2016**, *36*, 6051–6058.
- (14) Kumar, C. A.; Nagarajaprakash, R.; Victoria, W.; Veena, V.; Sakthivel, N.; Manimaran, B. *Inorg. Chem. Commun.* **2016**, *64*, 39–44.
- (15) Ye, R.-R.; Tan, C.-P.; Lin, Y.-N.; Ji, L.-N.; Mao, Z.-W. *Chem. Commun.* **2015**, *51*, 8353–8356.
- (16) Collery, P.; Mohsen, A.; Kermagoret, A.; Corre, S.; Bastian, G.; Tomas, A.; Wei, M.; Santoni, F.; Guerra, N.; Desmaële, D.; d'Angelo, J. *Invest. New Drugs* **2015**, *33*, 848–860.
- (17) Balakrishnan, G.; Rajendran, T.; Murugan, K. S.; Kumar, M. S.; Sivasubramanian, V. K.; Mahesh, A.; Thirunalasundari, T.; Rajagopal, S. *Inorg. Chim. Acta* **2015**, *434*, 51–59.
- (18) Medley, J.; Payne, G.; Banerjee, H. N.; Giri, D.; Winstead, A.; Wachira, J. M.; Krause, J. A.; Shaw, R.; Pramanik, S. K.; Mandal, S. K. *Mol. Cell. Biochem.* **2015**, *398*, 21–30.

- (19) Clède, S.; Lambert, F.; Saint-Fort, R.; Plamont, M. A.; Bertrand, H.; Vessières, A.; Policar, C. *Chem. - Eur. J.* **2014**, *20*, 8714–8722.
- (20) Coltery, P.; Bastian, G.; Santoni, F.; Mohsen, A.; Wei, M.; Coltery, T.; Tomas, A.; Desmaele, D.; D'Angelo, J. *Anticancer Res.* **2014**, *34*, 1679–1690.
- (21) Langdon-Jones, E. E.; Symonds, N. O.; Yates, S. E.; Hayes, A. J.; Lloyd, D.; Williams, R.; Coles, S. J.; Horton, P. N.; Pope, S. J. A. *Inorg. Chem.* **2014**, *53*, 3788–3797.
- (22) Kaplanis, M.; Stamatakis, G.; Papakonstantinou, V. D.; Paravatou-Petsotas, M.; Demopoulos, C. A.; Mitsopoulou, C. A. J. *Inorg. Biochem.* **2014**, *135*, 1–9.
- (23) Parson, C.; Smith, V.; Krauss, C.; Banerjee, H. N.; Reilly, C.; Krause, J. A.; Wachira, J. M.; Giri, D.; Winstead, A.; Mandal, S. K. *Br. J. Pharm. Res.* **2014**, *4*, 362–367.
- (24) Leonidova, A.; Pierroz, V.; Adams, L. A.; Barlow, N.; Ferrari, S.; Graham, B.; Gasser, G. *ACS Med. Chem. Lett.* **2014**, *5*, 809–814.
- (25) Wähler, K.; Ludewig, A.; Szabo, P.; Harms, K.; Meggers, E. *Eur. J. Inorg. Chem.* **2014**, *2014*, 807–811.
- (26) Kitanovic, I.; Can, S.; Alborzina, H.; Kitanovic, A.; Pierroz, V.; Leonidova, A.; Pinto, A.; Spingler, B.; Ferrari, S.; Molteni, R.; Steffen, A.; Metzler-Nolte, N.; Wölf, S.; Gasser, G. *Chem. - Eur. J.* **2014**, *20*, 2496–2507.
- (27) Leonidova, A.; Pierroz, V.; Rubbiani, R.; Heier, J.; Ferrari, S.; Gasser, G. *Dalton Trans.* **2014**, *43*, 4287–4297.
- (28) Yin Zhang, K.; Tso, K. K.-S.; Louie, M. W.; Liu, H. W.; Lo, K. K.-W. *Organometallics* **2013**, *32*, 5098–5102.
- (29) Redshaw, C.; Watkins, S.; Humphrey, S. M.; Bulman Page, P. C.; Ashby, S.; Chao, Y.; Herbert, C. J.; Mueller, A. *RSC Adv.* **2013**, *3*, 23963–23966.
- (30) Choi, A. W.-T.; Louie, M.-W.; Li, S. P.-Y.; Liu, H.-W.; Chan, B. T.-N.; Lam, T. C.-Y.; Lin, A. C.-C.; Cheng, S.-H.; Lo, K. K.-W. *Inorg. Chem.* **2012**, *51*, 13289–13302.
- (31) Lo, K. K.-W.; Zhang, K. Y.; Li, S. P.-Y. *Eur. J. Inorg. Chem.* **2011**, *2011*, 3551–3568.
- (32) Kermagoret, A.; Morgant, G.; d'Angelo, J.; Tomas, A.; Roussel, P.; Bastian, G.; Coltery, P.; Desmaële, D. *Polyhedron* **2011**, *30*, 347–353.
- (33) Rajagopalan, R.; Grummon, G. D.; Bugaj, J.; Hallemann, L. S.; Webb, E. G.; Marmion, M. E.; Vanderheyden, J. L.; Srinivasan, A. *Bioconjugate Chem.* **1997**, *8*, 407–415.
- (34) Takeda, H.; Ishitani, O. *Coord. Chem. Rev.* **2010**, *254*, 346–354.
- (35) Zobi, F.; Blacque, O.; Sigel, R. K. O.; Alberto, R. *Inorg. Chem.* **2007**, *46*, 10458–10460.
- (36) Zobi, F.; Spingler, B.; Alberto, R. *ChemBioChem* **2005**, *6*, 1397–1405.
- (37) Zobi, F.; Spingler, B.; Fox, T.; Alberto, R. *Inorg. Chem.* **2003**, *42*, 2818–2820.
- (38) Oriskovich, T. A.; White, P. S.; Thorp, H. H. *Inorg. Chem.* **1995**, *34*, 1629–1631.
- (39) Salignac, B.; Grundler, P. V.; Cayemittes, S.; Frey, U.; Scopelliti, R.; Merbach, A. E.; Hedinger, R.; Hegetschweiler, K.; Alberto, R.; Prinz, U.; Raabe, G.; Kölle, U.; Hall, S. *Inorg. Chem.* **2003**, *42*, 3516–3526.
- (40) Lo, K. K.-W. *Acc. Chem. Res.* **2015**, *48*, 2985–2995.
- (41) Clède, S.; Policar, C. *Chem. - Eur. J.* **2015**, *21*, 942–958.
- (42) Jürgens, S.; Herrmann, W. A.; Kühn, F. E. *J. Organomet. Chem.* **2014**, *751*, 83–89.
- (43) Kurz, P.; Probst, B.; Spingler, B.; Alberto, R. *Eur. J. Inorg. Chem.* **2006**, *2006*, 2966–2974.
- (44) Smieja, J. M.; Kubiak, C. P. *Inorg. Chem.* **2010**, *49*, 9283–9289.
- (45) Chan, C. Y.; Pellegrini, P. A.; Greguric, I.; Barnard, P. J. *Inorg. Chem.* **2014**, *53*, 10862–10873.
- (46) Gottschaldt, M.; Koth, D.; Müller, D.; Klette, I.; Rau, S.; Görls, H.; Schäfer, B.; Baum, R.; Yano, S. *Chem. - Eur. J.* **2007**, *13*, 10273–10280.
- (47) Domínguez, S. E.; Alborés, P.; Fagalde, F. *Polyhedron* **2014**, *67*, 471–480.
- (48) Tzeng, B.-C.; Chen, B.-S.; Chen, C.-K.; Chang, Y.-P.; Tzeng, W.-C.; Lin, T.-Y.; Lee, G.-H.; Chou, P.-T.; Fu, Y.-J.; Chang, A. H.-H. *Inorg. Chem.* **2011**, *50*, 5379–5388.
- (49) Coe, B. J.; Foxon, S. P.; Pilkington, R. A.; Sánchez, S.; Whittaker, D.; Clays, K.; Van Steerteghem, N.; Brunschwigg, B. S. *Organometallics* **2016**, *35*, 3014–3024.
- (50) Chiarella, G. M.; Cotton, F. A.; Dalal, N. S.; Murillo, C. A.; Wang, Z.; Young, M. D. *Inorg. Chem.* **2012**, *51*, 5257–5263.
- (51) Rodríguez, M. C.; Bravo, J.; Freijanes, E.; Oñate, E.; García-Fontán, S.; Rodríguez-Seoane, P. *Polyhedron* **2004**, *23*, 1045–1053.
- (52) Mella, P.; Cabezas, K.; Cerda, C.; Cepeda-Plaza, M.; Günther, G.; Pizarro, N.; Vega, A. *New J. Chem.* **2016**, *40*, 6451–6459.
- (53) Schutte, M.; Kemp, G.; Visser, H. G.; Roodt, A. *Inorg. Chem.* **2011**, *50*, 12486–12498.
- (54) Rillema, D. P.; Kirgan, R. A.; Smucker, B.; Moore, C. *Acta Crystallogr., Sect. E: Struct. Rep. Online* **2007**, *63*, m1404–m1405.
- (55) Connick, W. B.; Di Bilio, A. J.; Schaeffer, W. P.; Gray, H. B. *Acta Crystallogr., Sect. C: Cryst. Struct. Commun.* **1999**, *55*, 913–916.
- (56) Singh, A.; Anandhi, U.; Cinellu, M. A.; Sharp, P. R. *Dalton Trans.* **2008**, 2314–2327.
- (57) Hollis, L. S.; Lippard, S. J. *J. Am. Chem. Soc.* **1981**, *103*, 6761–6763.
- (58) Orsa, D. K.; Nettles, C. R.; Pramanik, S. K.; Iwunze, M. O.; Greco, G. E.; Krause, J. A.; Mandal, S. K. In *Handbook of Prostate Cancer Cell Research*; Nova Science: Hauppauge, 2009; pp 323–362.
- (59) *OECD Guidelines for the Testing of Chemicals*; OECD Publishing: Paris, 2004; pp 1–11.
- (60) Platts, J. A.; Oldfield, S. P.; Reif, M. M.; Palmucci, A.; Gabano, E.; Osella, D. *J. Inorg. Biochem.* **2006**, *100*, 1199–1207.
- (61) Shen, D.-W.; Akiyama, S.-I.; Schoenlein, P.; Pastan, I.; Gottesman, M. M. *Br. J. Cancer* **1995**, *71*, 676–683.
- (62) Akiyama, S.; Fojo, A.; Hanover, J. A.; Pastan, I.; Gottesman, M. M. *Somatic Cell Mol. Genet.* **1985**, *11*, 117–126.
- (63) Godwin, A. K.; Meister, A.; O'Dwyer, P. J.; Huang, C. S.; Hamilton, T. C.; Anderson, M. E. *Proc. Natl. Acad. Sci. U. S. A.* **1992**, *89*, 3070–3074.
- (64) Barr, M. P.; Gray, S. G.; Hoffmann, A. C.; Hilger, R. A.; Thomale, J.; O'Flaherty, J. D.; Fennell, D. A.; Richard, D.; O'Leary, J. J.; O'Byrne, K. J. *PLoS One* **2013**, *8*, e54193.
- (65) Robertazzi, A.; Platts, J. A. *JBIC, J. Biol. Inorg. Chem.* **2005**, *10*, 854–866.
- (66) Thorp-Greenwood, F. L.; Balasingham, R. G.; Coogan, M. P. *J. Organomet. Chem.* **2012**, *714*, 12–21.
- (67) Fernandez-Moreira, V.; Thorp-Greenwood, F. L.; Coogan, M. P. *Chem. Commun.* **2010**, *46*, 186–202.
- (68) Lo, K. K.-W.; Louie, M.-W.; Zhang, K. Y. *Coord. Chem. Rev.* **2010**, *254*, 2603–2622.
- (69) Fernández-Moreira, V.; Thorp-Greenwood, F. L.; Amoroso, A. J.; Cable, J.; Court, J. B.; Gray, V.; Hayes, A. J.; Jenkins, R. L.; Kariuki, B. M.; Lloyd, D.; Millet, C. O.; Williams, C. F.; Coogan, M. P. *Org. Biomol. Chem.* **2010**, *8*, 3888–3901.
- (70) Bucci, C.; Parton, R. G.; Mather, I. H.; Stunnenberg, H.; Simons, K.; Hoflack, B.; Zerial, M. *Cell* **1992**, *70*, 715–728.
- (71) Gillooly, D. J.; Morrow, I. C.; Lindsay, M.; Gould, R.; Bryant, N. J.; Gaullier, J. M.; Parton, R. G.; Stenmark, H. *EMBO J.* **2000**, *19*, 4577–4588.
- (72) Luzio, J. P.; Gray, S. R.; Bright, N. A. *Biochem. Soc. Trans.* **2010**, *38*, 1413–1416.
- (73) Luzio, J. P.; Pryor, P. R.; Bright, N. A. *Nat. Rev. Mol. Cell Biol.* **2007**, *8*, 622–632.
- (74) Kimura, S.; Noda, T.; Yoshimori, T. *Autophagy* **2007**, *3*, 452–460.
- (75) Senese, S.; Lo, Y. C.; Huang, D.; Zangle, T. A.; Gholkar, A. A.; Robert, L.; Homet, B.; Ribas, A.; Summers, M. K.; Teitell, M. A.; Damoiseaux, R.; Torres, J. Z. *Cell Death Dis.* **2014**, *5*, e1462.
- (76) Morgan, D. *The Cell Cycle: Principles of Control*; Lawrence, E., Ed.; Sinauer Associates: London, 2007.
- (77) Zhang, D.; Piao, H.-L.; Li, Y.-H.; Qiu, Q.; Li, D.-J.; Du, M.-R.; Tsang, B. K. *Exp. Mol. Pathol.* **2016**, *100*, 506–513.

- (78) Swift, L. H.; Golsteyn, R. M. *Biol. Cell* **2016**, *108*, 127–148.
- (79) van Engeland, M.; Nieland, L.; Ramaekers, F.; Schutte, B.; Reutelingsperger, C. *Cytometry* **1998**, *31*, 1–9.
- (80) Mizukami, S.; Kikuchi, K.; Higuchi, T.; Urano, Y.; Mashima, T.; Tsuruo, T.; Nagano, T. *FEBS Lett.* **1999**, *453*, 356–360.
- (81) Zamzami, N.; Marchetti, P.; Castedo, M.; Decaudin, D.; Macho, A.; Hirsch, T.; Susin, S. A.; Petit, P. X.; Mignotte, B.; Kroemer, G. *J. Exp. Med.* **1995**, *182*, 367–377.
- (82) Kluck, R. M.; Bossy-Wetzel, E.; Green, D. R.; Newmeyer, D. D. *Science* **1997**, *275*, 1132–1136.
- (83) Maltese, W. A.; Overmeyer, J. H. *Am. J. Pathol.* **2014**, *184*, 1630–1642.
- (84) Yoon, M. J.; Lee, A. R.; Jeong, S. A.; Kim, Y.-S.; Kim, J. Y.; Kwon, Y.-J.; Choi, K. S. *Oncotarget* **2014**, *5*, 6816–6831.
- (85) Li, B.; Zhao, J.; Wang, C.-Z.; Searle, J.; He, T.-C.; Yuan, C.-S.; Du, W. *Cancer Lett.* **2011**, *301*, 185–192.
- (86) Guicciardi, M. E.; Leist, M.; Gores, G. J. *Oncogene* **2004**, *23*, 2881–2890.
- (87) Kieran, D.; Greensmith, L. *Neuroscience* **2004**, *125*, 427–439.
- (88) Suntharalingam, K.; Awuah, S. G.; Bruno, P. M.; Johnstone, T. C.; Wang, F.; Lin, W.; Zheng, Y.-R.; Page, J. E.; Hemann, M. T.; Lippard, S. J. *J. Am. Chem. Soc.* **2015**, *137*, 2967–2974.
- (89) Flamme, M.; Cressey, P. B.; Lu, C.; Bruno, P. M.; Eskandari, A.; Hemann, M. T.; Hogarth, G.; Suntharalingam, K. *Chem. - Eur. J.* **2017**, *23*, 9674–9682.
- (90) Moriwaki, K.; Bertin, J.; Gough, P. J.; Orlowski, G. M.; Chan, F. K. M. *Cell Death Dis.* **2015**, *6*, e1636.
- (91) Boulares, A. H.; Yakovlev, A. G.; Ivanova, V.; Stoica, B. A.; Wang, G.; Iyer, S.; Smulson, M. J. *Biol. Chem.* **1999**, *274*, 22932–22940.
- (92) Tanida, I.; Ueno, T.; Kominami, E. In *Autophagosome and Phagosome*; Deretic, V., Ed.; Humana Press: Totowa, NJ, 2008; pp 77–88.
- (93) Wang, W. B.; Feng, L. X.; Yue, Q. X.; Wu, W. Y.; Guan, S. H.; Jiang, B. H.; Yang, M.; Liu, X.; Guo, D. A. *J. Cell. Physiol.* **2012**, *227*, 2196–2206.
- (94) Tripathy, S. K.; De, U.; Dehury, N.; Laha, P.; Panda, M. K.; Kim, H. S.; Patra, S. *Dalton Trans.* **2016**, *45*, 15122–15136.
- (95) Puckett, C. A.; Ernst, R. J.; Barton, J. K. *Dalton Trans.* **2010**, *39*, 1159–1170.
- (96) Shoemaker, R. H. *Nat. Rev. Cancer* **2006**, *6*, 813–823.
- (97) Lira-Puerto, V.; Silva, A.; Morris, M.; Martinez, R.; Groshen, S.; Morales-Canfield, F.; Tenorio, F.; Muggia, F. *Cancer Chemother. Pharmacol.* **1991**, *28*, 391–396.
- (98) Huang, R.; Wallqvist, A.; Covell, D. G. *Biochem. Pharmacol.* **2005**, *69*, 1009–1039.
- (99) Leonidova, A.; Gasser, G. *ACS Chem. Biol.* **2014**, *9*, 2180–2193.
- (100) Louie, M.-W.; Liu, H.-W.; Lam, M. H.-C.; Lau, T.-C.; Lo, K. K.-W. *Organometallics* **2009**, *28*, 4297–4307.
- (101) Egli, A.; Hegetschweiler, K.; Alberto, R.; Abram, U.; Schibli, R.; Hedinger, R.; Gramlich, V.; Kissner, R.; Schubiger, P. A. *Organometallics* **1997**, *16*, 1833–1840.
- (102) Orsa, D. K.; Haynes, G. K.; Pramanik, S. K.; Iwunze, M. O.; Greco, G. E.; Ho, D. M.; Krause, J. A.; Hill, D. A.; Williams, R. J.; Mandal, S. K. *Inorg. Chem. Commun.* **2008**, *11*, 1054–1056.
- (103) Huang, H.; Humbert, N.; Bizet, V.; Patra, M.; Chao, H.; Mazet, C.; Gasser, G. *J. Organomet. Chem.* **2017**, *839*, 15–18.
- (104) Hall, M. D.; Telma, K. A.; Chang, K.-E.; Lee, T. D.; Madigan, J. P.; Lloyd, J. R.; Goldlust, I. S.; Hoeschele, J. D.; Gottesman, M. M. *Cancer Res.* **2014**, *74*, 3913–3922.
- (105) Ferreira, J. A.; Peixoto, A.; Neves, M.; Gaiteiro, C.; Reis, C. A.; Assaraf, Y. G.; Santos, L. L. *Drug Resist. Updates* **2016**, *24*, 34–54.
- (106) Giaccone, G. *Drugs* **2000**, *59*, 9–17.
- (107) Jovanović, S.; Petrović, B.; Bugarčić, Ž. D. *J. Coord. Chem.* **2010**, *63*, 2419–2430.
- (108) Zobi, F.; Spingler, B. *Inorg. Chem.* **2012**, *51*, 1210–1212.
- (109) Santoro, G.; Blacque, O.; Zobi, F. *Metallomics* **2012**, *4*, 253–259.
- (110) Binkley, S. L.; Leeper, T. C.; Rowlett, R. S.; Herrick, R. S.; Ziegler, C. J. *Metallomics* **2011**, *3*, 909–916.
- (111) Miller, J. E.; Grădinaru, C.; Crane, B. R.; Di Bilio, A. J.; Wehbi, W. A.; Un, S.; Winkler, J. R.; Gray, H. B. *J. Am. Chem. Soc.* **2003**, *125*, 14220–14221.
- (112) Tavaré, R.; Williams, J.; Howland, K.; Blower, P. J.; Mullen, G. E. D. *J. Inorg. Biochem.* **2012**, *114*, 24–27.
- (113) Ye, R.-R.; Tan, C.-P.; Chen, M.-H.; Hao, L.; Ji, L.-N.; Mao, Z.-W. *Chem. - Eur. J.* **2016**, *22*, 7800–7809.
- (114) Ghosh, K.; De, S.; Das, S.; Mukherjee, S.; Sengupta Bandyopadhyay, S. *PLoS One* **2016**, *11*, e0168488.
- (115) Wang, Y.; Zhu, X.; Yang, Z.; Zhao, X. *Biochem. Biophys. Res. Commun.* **2013**, *430*, 876–882.
- (116) Xue, X.; Piao, J.-H.; Nakajima, A.; Sakon-Komazawa, S.; Kojima, Y.; Mori, K.; Yagita, H.; Okumura, K.; Harding, H.; Nakano, H. *J. Biol. Chem.* **2005**, *280*, 33917–33925.
- (117) Matsuyama, S.; Llopis, J.; Deveraux, Q. L.; Tsien, R. Y.; Reed, J. C. *Nat. Cell Biol.* **2000**, *2*, 318–325.
- (118) Lemasters, J. J.; Nieminen, A.-L.; Qian, T.; Trost, L. C.; Elmore, S. P.; Nishimura, Y.; Crowe, R. A.; Cascio, W. E.; Bradham, C. A.; Brenner, D. A.; Herman, B. *Biochim. Biophys. Acta, Bioenerg.* **1998**, *1366*, 177–196.
- (119) Sawai, H.; Domae, N. *Biochem. Biophys. Res. Commun.* **2011**, *411*, 569–573.
- (120) Sun, Q.; Chen, T.; Wang, X.; Wei, X. *J. Cell. Physiol.* **2010**, *222*, 421–432.
- (121) Martínez-Lillo, J.; Mastropietro, T. F.; Lappano, R.; Madeo, A.; Alberto, M. E.; Russo, N.; Maggiolini, M.; De Munno, G. *Chem. Commun.* **2011**, *47*, 5283–5285.
- (122) Pho, M. T.; Ashok, A.; Atwood, W. J. *J. Virol.* **2000**, *74*, 2288–2292.
- (123) Louie, M.-W.; Liu, H.-W.; Lam, M. H.-C.; Lam, Y.-W.; Lo, K. K.-W. *Chem. - Eur. J.* **2011**, *17*, 8304–8308.
- (124) Martin, C. J.; Gaisser, S.; Challis, I. R.; Carletti, I.; Wilkinson, B.; Gregory, M.; Prodromou, C.; Roe, S. M.; Pearl, L. H.; Boyd, S. M.; Zhang, M.-Q. *J. Med. Chem.* **2008**, *51*, 2853–2857.
- (125) Wehrli, W.; Knüsel, F.; Schmid, K.; Staehelin, M. *Proc. Natl. Acad. Sci. U. S. A.* **1968**, *61*, 667–673.
- (126) Blagg, B. S. J.; Kerr, T. D. *Med. Res. Rev.* **2006**, *26*, 310–338.
- (127) Khajapeer, K. V.; Baskaran, R. *Leuk. Res. Treat.* **2015**, *2015*, 1–16.
- (128) Holzbeierlein, J. M.; Windsperger, A.; Vielhauer, G. *Curr. Oncol. Rep.* **2010**, *12*, 95–101.
- (129) Davenport, J.; Balch, M.; Galam, L.; Girgis, A.; Hall, J.; Blagg, B. S. J.; Matts, R. L. *Biology* **2014**, *3*, 101–138.
- (130) Alberto, R. *Eur. J. Inorg. Chem.* **2009**, *2009*, 21–31.
- (131) Yazdani, A.; Janzen, N.; Czorny, S.; Valliant, J. F. *Inorg. Chem.* **2017**, *56*, 2958–2965.
- (132) Yazdani, A.; Janzen, N.; Banevicius, L.; Czorny, S.; Valliant, J. F. *Inorg. Chem.* **2015**, *54*, 1728–1736.